Int. J. Electrochem. Sci., 13 **(2018)** 11648 – 11662, doi: 10.20964/2018.12.75

International Journal of ELECTROCHEMICAL SCIENCE
www.electrochemsci.org

Structural and Electrical Investigation of New Melilite Compound $K_{0.86}Na_{1.14}CoP_2O_7$

Riadh Marzouki[1,2,*], *Youssef Ben Smida*[3], *Abderrahmen Guesmi*[2], *Samuel Georges*[4], *Ismat H. Ali*[1], *Stefan Adams*[5], *Mohamed Faouzi Zid*[2]

[1] Chemistry Department, College of Science, King Khaled University, Abha 61413, Saudi Arabia.
[2] Laboratory of Materials, Crystallochemistry and Applied Thermodynamics, Faculty of Sciences of Tunis, University of Tunis El Manar, Tunisia.
[3] National Center of Materials Sciences Research, Technopole Borj Cedria, 8027 Soliman, Tunisia.
[4] CNRS, LEPMI, F-38000 Grenoble, France.
[5] Department of Materials Science and Engineering, Faculty of Engineering, National University of Singapore, Singapore.
[*]E-mail: riadh.marzouki@hotmail.fr

Received: 11 September 2018 / *Accepted:* 2 October 2018 / *Published:* 5 November 2018

A new sodium-potassium cobalt diphosphate, $K_{0.86}Na_{1.14}CoP_2O_7$, is synthesized by solid state reaction method and characterized by X-ray diffraction (XRD) and impedance spectroscopy. The resulting structural model is supports by bond-valence-sum analysis (BVS) and charge distribution validations (CHARDIT) tools. The mixed pyrophosphate crystallizes in the tetragonal system, space group $P4_2/mnm$ with a=7.808(3) Å, c=10.757(3) Å. The structure is described as a 2D anionic framework with alkali cations sandwiched between layers. As mechanical grinder, ball-milling was used in order to reduce average particle size of the prepared powder. The optimal sintering temperature of the ceramic is 560°C, leading to a relative density of 83%. Their microstructure is characterized by scanning electron microscopy (SEM). The conductivity measurements of the obtained ceramic are studied over a temperature range from 360°C to 480°C. It shows that $K_{0.86}Na_{1.14}CoP_2O_7$ material is a low ionic conductor with a conductivity of $\sigma = 8.26\times10^{-7}$ $S.cm^{-1}$ at 390°C and an activation energy of 1.34 eV. The bond valence site energy (BVSE) model is used to identify the conduction pathways for the monovalent cations, allowing a better correlation between the electrical and the structural data.

Keywords: Crystal structure; relative density; microstructure; impedance spectroscopy; conduction pathways.

1. INTRODUCTION

Recently, a huge number of materials with general formula $A_2MP_2O_7$ (A: monovalent cation, M: transition metal cation) with diverse structure types were reported in the bibliography [1-9]. The investigations of these materials concerned the synthesis, the structural features and the physical properties (electrical, magnetic, optical …). Impedance spectroscopy showed that most of these materials are purely cationic conductors [1,4]; whereas some other phases are mixed conductors with substantial contributions of the electronic components to the total conductivity [8].

For $A_2MP_2O_7$ phases with M = Co, the structure and the electrical properties of the tetragonal $Na_2CoP_2O_7$ phosphate have been reported by Sanz [1]. Guesmi [9] reported the structure of the isostructural K-Co phase. Their melilite-related structure [10] is formed by $[CoP_2O_7]^{-2}{}_{\infty}$ slabs – with alkali cations located between the layers. The anionic framework presents two independent crystallographic positions for the alkali cations. In order to study the alkali distribution over these positions, the structure of $K_{0.86}Na_{1.14}CoP_2O_7$ with intermediate composition has been determined by single crystal X-ray diffraction. The second purpose of this investigation is to examine the electrical properties of the title compound. In the tetragonal form, only one $Na_2CoP_2O_7$ has so far been electrically characterized [1]. The monovalent ions conduction pathways in the crystal structures were simulated using the bond valence sum energy model, allowing a better correlation between the electrical and the structural features, mainly the cationic substitution.

2. EXPERIMENTAL

2.1. Single crystal and polycrystalline material preparation

$K_{0.86}Na_{1.14}CoP_2O_7$ was prepared by slow evaporation of aqueous solution of high-purity reagents KNO_3 (≥ 99%, Fluka), $NaNO_3$ (≥ 99%, Fluka), $NH_4H_2PO_4$ (≥ 99%, Fluka) and $Co(NO_3)_2.6H_2O$ (99%, Aldrich) with K:Na:Co:P molar ratio of 1:1:1:2. After evaporation, the mixture is placed in silica crucible. To eliminate volatile products, it was ground and slowly annealed to 400°C for 12h, in air. After that, the sample was progressively heated at 660°C for 4 days and-slowly cooled down to room temperature at $5°C.h^{-1}$. The obtained blue crystals were isolated by washing the residue in boiling water. A qualitative EDS analysis (energy-dispersive X-ray spectroscopy) detected the K, Na, Co, P and Oxygen elements.

A polycrystalline powder of $K_{0.86}Na_{1.14}CoP_2O_7$ was prepared by a treatment of the stoichiometric mixture of the above noted regents. In fact, the powder XRD pattern was in convenient agreement with single-crystal structure. The resulting phase is stable under ambient conditions and their synthesis reproducible. The synthesis details are described in previous works [11].

2.2. Characterizations

Qualitative analysis by scanning electron microscopy probe (SEM) was operated via a Philips XL 30 type apparatus.

An adequate single crystal, with $0.21 \times 0.21 \times 0.17$ mm^3 dimensions, was selected for the structure determination. The structural data were collected, at room temperature, on an Enraf-Nonius CAD-4 [12-13] diffractometer using the MoKα (λ=0.71073Å) radiation. The ordinary corrections; for

Lorentz and polarization effects, absorption via a psi-scan [14] and secondary extinction correction [15] were applied. All subsequent calculations were carried out using the SHELX-97 [15] computer programs included in the WinGX software package [16]. Structure graphics were figured with Diamond 2.1 program [17]. A summary of the fundamental crystal data is given in Table 1.

Table 1. Summary of crystallographic data, recording conditions and structure refinement results for $K_{0.86}Na_{1.14}CoP_2O_7$.

Crystal data	
Empirical formula	$K_{0.86}Na_{1.14}CoP_2O_7$
Crystal shape ; color	Parallelepiped ; blue
Crystal size	0.25×0.25×0.22 mm^3
Crystal system ; space group	Tetragonal ; $P\ 4_2/m\ n\ m$
Unit cell dimensions	a=7.808(3) Å, c=10.757(3) Å,
Volume ; Z	655.8(4) $Å^3$, 4
Formula weight ; ρ_{calc}	292.73 $g.mol^{-1}$; 2.965 $g.cm^{-3}$
Absorption coefficient (μ)	3.717 mm^{-1}
Data collection	
Diffractometer	Enraf-Nonius CAD-4
Wavelength ; temperature	$\lambda_{Mo\ K\alpha}$ = 0.71069Å; 298(2) K
Theta range for data collection	$3.22 \leq \theta \leq 26.94°$
Limiting Indices	$-9 \leq h \leq 9$, $-1 \leq k \leq 9$, $-1 \leq l \leq 13$
Collected reflections	1834
Independent reflections	418 [R_{int} = 0.0888]
Observed reflections [I>2σ(I)]	298
Refinement	
Refinement method	Full-matrix least-squares on F^2
Final R indices [I>2σ(I)]	R=0.0353 ; wR=0.0623
Reflections / parameters / restraints	418 / 41 / 2
$\Delta\rho_{max}$; $\Delta\rho_{min}$ (e.$Å^{-3}$)	0.60 / -0.45
Extinction coefficient; S	0.009(2)
Goodness of fit (S)	1.03

Using a Philips D8 diffractometer operating with Cu anticathode K_α (λ=1.5406 Å), X-ray powder diffraction pattern was recorded in a range of 2θ=[10°-70°] with step 0.02°, at room temperature.

As to the electrical studies, the measurements were preceded by a pretreatment of sample in order to reduce the mean particle size of the obtained powder. For this reason, the sample underwent a ball-grinding using a planetary micromill pulverisette apparatus (FRITSCH) equipped with agate balls into ethanol and agate jars. For ball milling, six agate balls and 5 grams of powder are putted in the agate jar. The milling was carried out in ethanol to avoid pollution and undue heating during the experiment. Alternation of 10 min milling series with 5 min break ones have been applied for 150 min total duration of the experiment. It should be noted that during the last 3 grinding sequences, volume densities of the material have not increased. For this reason, we finished grinding. Indeed, despite of the presence addition of ethanol, milling operation remains an energetic process; it causes enough heating of the whole machine. Thus, the pause suite enable the system to cool down after each milling sequence. After sintering at 600 °C, we have increased the volume density of the material to exceed 80%. The values of relative volume density of the material before and after grinding are 77 % and 83 %, respectively. They were determined from accurate measurements of the samples sizes and mass, with comparison to the theoretical density deduced from the crystal structure.

Impedance spectroscopy measurements were performed in a HP 4192-A automatic bridge controlled by a microcomputer. With a 0.5V ac signal, impedance spectra were recorded in 13MHz-50Hz frequency range within the 360-480°C temperature range with measurements taken in steps of 30° C. The sample was pelletized by uniaxial shaping accomplished by isostatic pressing at 2.5kbar. Then, it sintered, in air, for 2h at 540°C. The heating and cooling rates are 5K.min-^{1}. The surface and thickness of pellet was about 0.5 cm^{2} and 4 mm, respectively. Platinum electrodes were connected to the two faces of the pellet via a platinum paste to keep good electric contacts, and then painted pellet was carried out at steady-state temperatures in still air.

For SEM observation, sintered pellet was polished and thermally etched for 30 min 50K underneath the sintering temperature with heating/cooling rates of 5K.min^{-1}. Before SEM analysis which was performed using Philips XL 30 microscope, a gold layer was deposited by sputtering.

3. TRANSPORT PATHWAYS SIMULATION

The concept of bond valence [18,19] commonly used to validate the plausibility of crystal structure determination was successfully employed to model lithium ion conductivity in a variety of compounds such as $La_{2/3x}Li_{3x}TiO_3$ [20, 21], $LiFePO_4$ [22], sodium in NaSICON conductors [23] and $NaCo_2As_3O_{10}$ triarsenate [24], fluoride anion conductors [21] or to screen the ICSD database for new alkali ion conductors [25], etc. While bond valences $s_{A\text{-}X} = exp[(R_0 - R_{A\text{-}X}) / b]$ for the interaction between an anion X and a cation A, also their mismatches are primarily expressed randomly “valence units”. Recently, they may shown [29] also be related to an absolute energy scale by expressing the bond valence as a Morse-type interaction energy. For details see [26]. Briefly, the pathway approach defines regions with low site energy E(A) :

$$E(A) = D_0\left[\sum_{i=1}^{N}\left(\frac{s_{A-X_i} - s_{\mathrm{min},A-X_i}}{s_{\mathrm{min},,A-X_i}}\right)^2 - N\right] + E_{\mathrm{Coulomb}}\,(A-B) \qquad (1)$$

as regions that the mobile cation A can reach with an activation energy related to the value of E(A). For the purpose of such a transport pathway analysis by means of *bond-valence site energy* landscapes, it has proven useful to consider among the Coulomb repulsions of the mobile cation only those with the immobile cation types B so that collective motions of mobile ions can be captured. In both event Coulomb repulsions are filtered by an error function complement term

$$E_{\mathrm{Coulomb}}(A-B) \;=\; 14.4\,\frac{\mathrm{eV}}{\text{Å}}\,\frac{z_A \cdot z_B}{R_{A-B}}\,\mathrm{erfc}\left(\frac{R_{A-B}}{\rho_0}\right) \qquad (2)$$

and the fractional ion charges z_A, z_B are derived from the nominal charges and principal quantum numbers by the formalism explained in [26,27]. The terms of Coulomb attractions are mostly integrated in the Morse attraction term.

4. RESULTS AND DISCUSSION

4.1. Crystal Structure determination

The cobalt and phosphorus atoms were detected first and then oxygen atoms by successive Fourier difference synthesis. The two alkali cations positions (called hereinafter A1 and A2) were also identified and their positions refined according to their interatomic distances as occupied by the potassium for one and sodium for the other. When all the atoms except alkali ones were refined anisotropically, the agreement reliability factor converged to R=0.05. However, the highest peak and the deepest hole in the difference Fourier map are near the alkali positions implying a positional disorder over them. This suggestion was supported by the fact that their refined occupations deviate from a full occupancy. For these reasons, the two positions were refined as simultaneously occupied by the two cations leading to a smooth convergence of the reliability factors. The result corresponds to the empirical formula $K_{0.86}Na_{1.14}CoP_2O_7$. The crystallographic data summary of the title compound, especially conditions and structure refinement results, is shown at Table 1.

The obtained structural model was propped by both Bond valence sum model BVS [18,19] and charge distribution method CD [28,29] validation tools as the valences V according to the BVS model and charges Q from the CD analysis are in agreement with the formal oxidation numbers (Table 2). The atomic coordinates, isotropic displacement parameters and fractional occupancies are tabulated in Table 2.

Table 2. Atomic coordinates, equivalent isotropic thermal factors and BVS (V) and CD (Q) validation results in $K_{0.86}Na_{1.14}CoP_2O_7$.

Atom	**Position**	**x**	**y**	**z**	**U_{eq} (Å^2)**	**V ; Q**
Co	*4d*	½	0	1/4	0.0250(4)	1.96; 1.985
P	*16k*	0.6369(1)	0.3631(1)	0.2135(2)	0.0229(4)	4.98; 5.001
A1 $^{\Psi}$	*16k*	0.8090(3)	0.1910(3)	1/2	0.0316(11)	1.09; 1.009
A2 $^{\Psi}$	*8i*	0.8537(2)	0.1463(2)	0	0.0249(9)	1.03; 1.003
O1	*16k*	0.6379(4)	0.3621(4)	0.35138(4)	0.0332(11)	-1.91; -1.950
O2	*16k*	0.5770(4)	0.1974(4)	0.1522(3)	0.0369(9)	-1.97; -2.015
O3	*8j*	½	½	0.1636(7)	0.0534(22)	-2.34; -2.041

A1$^{\Psi}$: $K_{0.28(2)}Na_{0.72(2)}$; A2$^{\Psi}$: $K_{0.58(2)}Na_{0.42(2)}$; V: valence value, Q= charge value

The Rietveld refinement was carried out in the range 10-70° using the single crystal structure (Figure 1). The Rietveld refinement was executed using Janna computer software [30]. The final agreement factors are Rp=0.01, Rwp=0.012 and R(F^2)=0.081.

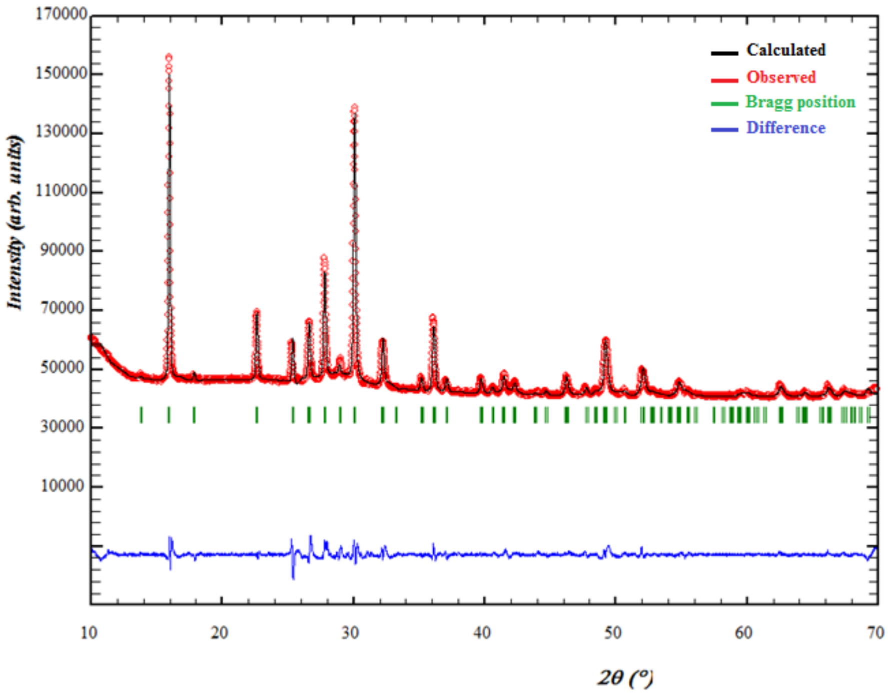

Figure 1. Rietveld refinement patterns of $K_{0.86}Na_{1.14}CoP_2O_7$

4.2. Structure analysis and description

The projection of the structure down the [100] direction in Figure 2 depicts the layer-like aspect of the structure with two alternating orientations of $[CoP_2O_7]^{2-}$ anion sheets per unit cell parallels to the *ab* plane, alkali cations are sandwiched between layers. Each $[CoP_2O_7]^{2-}$ plane (Figure 2) is composed of tetrahedrally coordinated cobalt ions connected to four diphosphate groups to form five-membered rings of 2 $[CoO_{4/2}]^{2-}$ and 3 $[PO_{3/2}O]$.

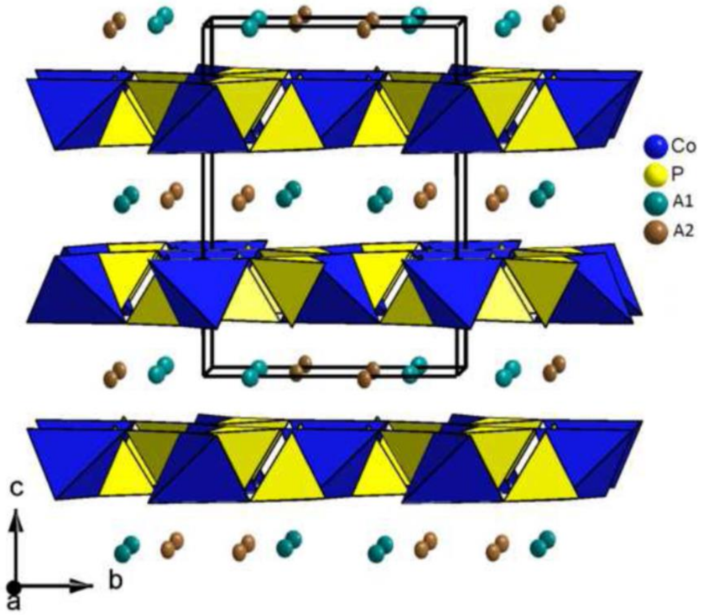

(a)

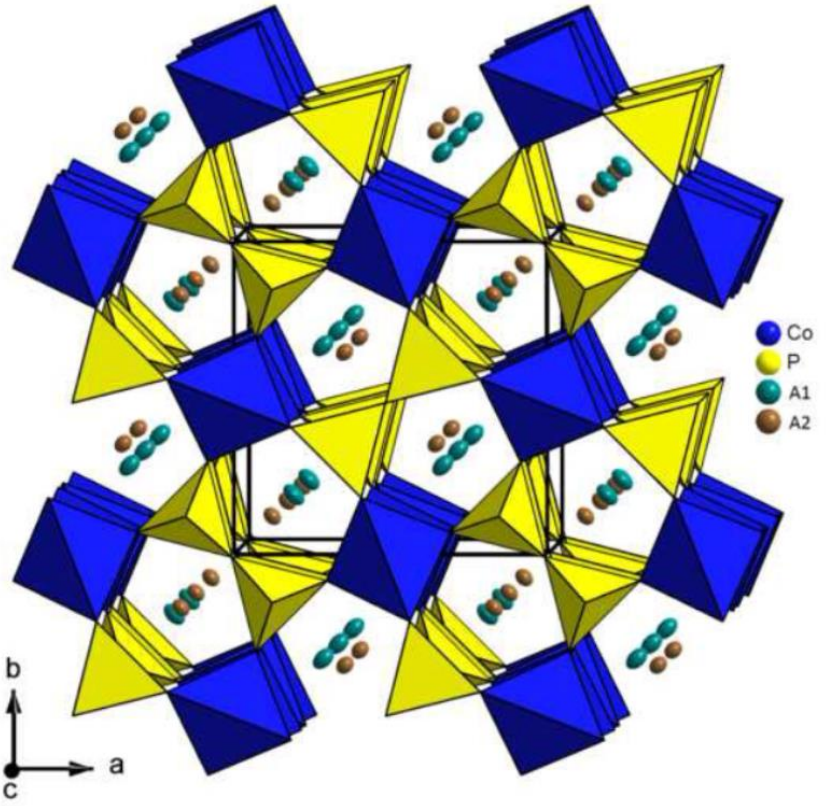

(b)

Figure 2. Polyhedral representation of the structure of $K_{0.86}Na_{1.14}CoP_2O_7$ showing the layer-like aspect of the framework parallel to [110] (a) and the tetrahedral sheet (b) near [001].

The alkali metal cations forming the second type of sheets appear above and below the pentagonal rings. Each of the two alkali positions is coordinated to eight oxygen atoms with bond distances ranging from 2.48 to 2.80 Å for the A1 site of the sodium-richest composition (A1: $K_{0.28}Na_{0.72}$) and all about 2.74 Å for the A2 site with near K/Na occupations (A2: $K_{0.58}Na_{0.42}$); the arithmetic mean A-O distances are consequently different.

4.3. Impedance spectroscopy analysis

Alternations of 10 min milling sequences have been executed for 150 min total duration of the experiment. At the optimal sintering temperature of 600 °C, an increase of the relative density of the material to from 77% (not milled) to 83% was obtained. The electrical properties were investigated from the sample of 83% of relative density. In anterior study, it is observed that porosity about 15% is answerable for only a slight augmentation of the measured conductivity [31].

The SEM micrograph of sintered $K_{0.86}Na_{1.14}CoP_2O_7$ pellet shows a good homogeneity of the grains with average sizes of about 3 μm (Figure 3). The residual porosity, figured in the micrograph, is thereabouts 17% whereas a good coalescence between grains is obtained.

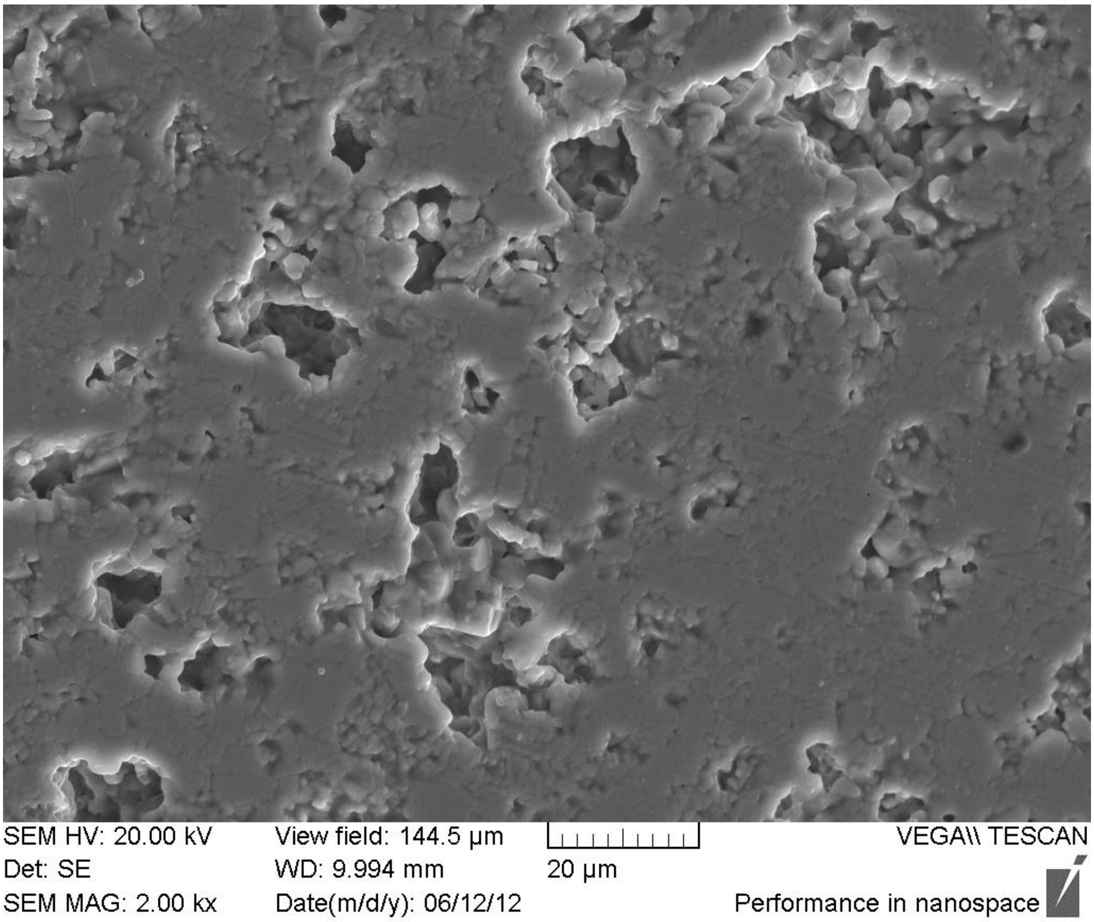

Figure 3. SEM micrograph of sintered $K_{0.86}Na_{1.14}CoP_2O_7$ pellet with relative density 83%.

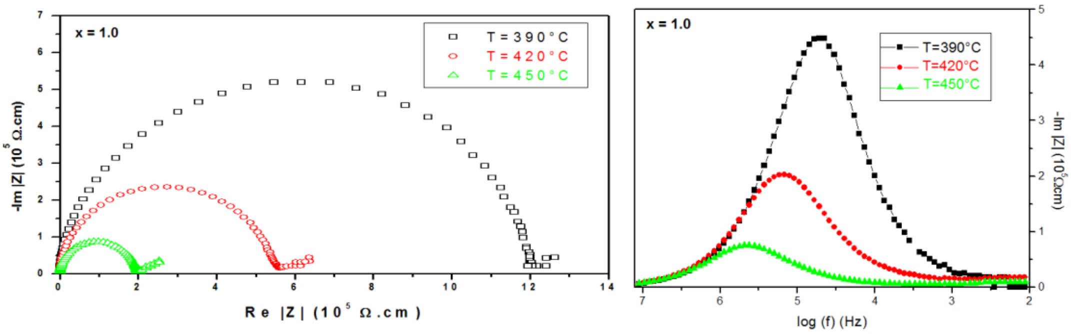

(a) **(b)**

Figure 4. Normalized complex impedance spectra recorded of $K_{0.86}Na_{1.14}CoP_2O_7$ sample at selected temperatures (a) Nyquist plane; (b) Bode plane.

The Nyquist plots for $K_{0.86}Na_{1.14}CoP_2O_7$ samples, at different temperatures, are shown in Figure 4. Zview software [32] was used to fit plots. In high frequency domain, the impedance diagrams show only one typical semicircle arc. An equivalent circuit collected a resistor R connected in parallel with a constant phase element CPE is used. The latter contribution is an empirical impedance function of the type:

$Z(\omega)_{CPE} = 1/C(j\omega)^p$; $(-1 \leq p \leq 1)$ (4)

At low frequencies (f ≤ 20Hz), a minor contribution is spotted; it is tentatively assigned to interfacial phenomena related to the electrode reaction [33], and not investigated further.

Fitted values of different electric parameters for $K_{0.86}Na_{1.14}CoP_2O_7$ compound, at different temperatures, are illustrated in Table 3. Accordingly, resistivities are extracted from the refinements as the one high frequency contributions.

Table 3. Electrical values of the equivalent circuit parameters calculated for $K_{0.86}Na_{1.14}CoP_2O_7$ sample at different temperatures.

T (°C)	**R (×10^5 Ω.cm)**	**C (×10^{-12} F)**	**p**
360	33.1	6.76	0.9
390	12.1	9.08	0.9
420	5.5	8.74	0.9
450	2.0	8.09	0.9
480	0.9	7.86	0.9

Linear Arrhenius plot of log(σT(S.Kcm^{-1})) vs. 10^3/T (K^{-1}), collected within the (360-480 °C) temperature range, are given in Figure 5. Following the Arrhenius law, the obtained activation energy of $K_{0.86}Na_{1.14}CoP_2O_7$ sample is 1.34 eV. The conductivity value σ at 390°C is $\sigma = 8.26\times10^{-7}$ S.cm^{-1}.

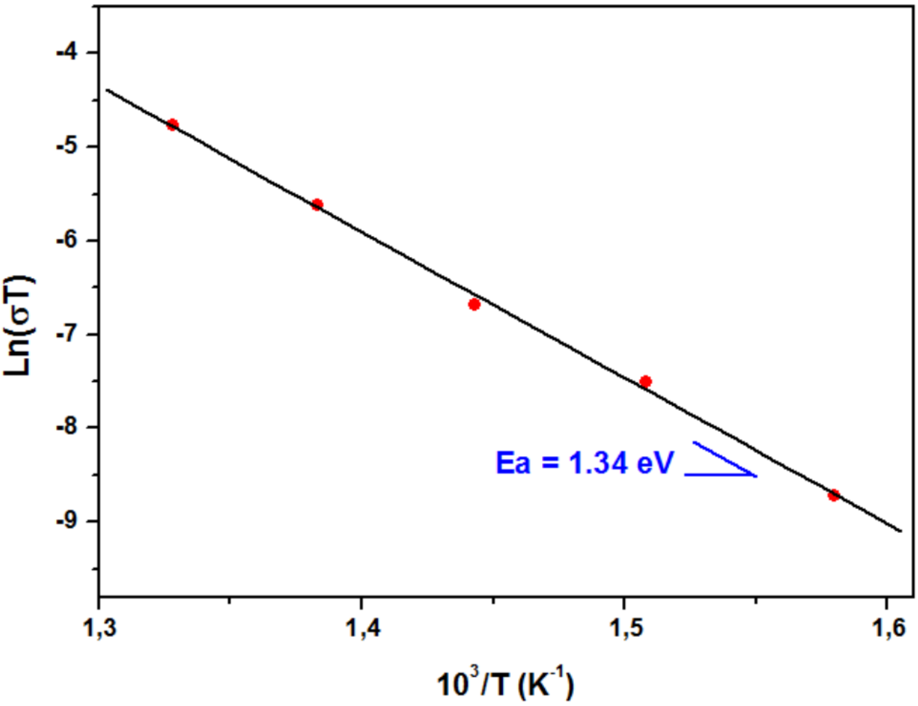

Figure 5. Arrhenius plot of of $K_{0.86}Na_{1.14}CoP_2O_7$.

Compared to some activation energies observed in diphosphates $Na_2CoP_2O_7$ (Ea=0.61 eV) [1], $NaAgZnP_2O_7$ (Ea=0.76 eV) [3], $Na_2PbP_2O_7$ (Ea=0.90 eV) [34], $Ag_2PbP_2O_7$ (Ea=0.78 eV) [35], $Na_{0.71}Ag_{0.29}CoP_2O_7$ (Ea=1.37 eV) [4], and in other materials such as $Na_4Co_{5.63}Al_{0.91}(AsO_4)_6$ (Ea=0.93 eV) [36], $Na_4Co_7(AsO_4)_6$ (Ea=1.0 eV) [37], $Na_2Co_2(MoO_4)_3$ (Ea=1.2 eV) [38], $K_{0.86}Na_{1.14}CoP_2O_7$ exhibits a low electrical conductivity. Hence, the influence of cationic substitution in the tetragonal phase can be clearly observed. In fact, the activation energy increases from 0.61 eV in $Na_2CoP_2O_7$ [1] to 1.34 eV in $K_{0.86}Na_{1.14}CoP_2O_7$. Also, the value of conductivity decreases from 3×10^{-5} $S.cm^{-1}$ at 300°C in $Na_2CoP_2O_7$ [1] to 8.26×10^{-7} $S.cm^{-1}$ at 390°C in $K_{0.86}Na_{1.14}CoP_2O_7$ material. This effect was confidently attributed to chemical composition.

4.4. Conduction pathways proposed from bond valence analysis

It is supposed that *dc* conduction necessitates continuous pathways that traverse the unit cell in minimum one direction. In fact, these pathways are displayed as regions enclosed by isosurfaces of constant site energy *E*(Na). A grid of 144^3 points was used and *E*(Na) was calculated for each grid point as a hypothetical Na position. The threshold value of *E*(Na) for which the *E*(Na) isosurfaces shape visualized a continuous migration pathway (including both vacant and occuped Na sites), permits a rough estimate of the activation energy for theNa^+ ion transport process. Since an approach neglects relaxation, the assessment of the activation energy is based on an empirical correlation observed for a wide range of cation conductors.

4.4.1. Na transport pathways in $Na_2CoP_2O_7$

Sodium ion transport pathways for the single alkali composition $Na_2CoP_2O_7$ can be predicted from the literature crystal structure determination [1] as paths of low bond valence site energy. As ion transport in this compound is found to be restricted to a two-dimensional transport within the alkali ion layer, only the projection of half a unit cell along *c* on the *ab* plane is shown here in Figure 7. In this graph three superimposed isosurfaces of constant Na^+ site energy illustrate the sites, local pathways and infinite pathways for *dc* ionic conductivity. The equilibrium sites Na(1) and Na(2) represent the minima of the bond valence site energy maps with site energies *E*(Na,2) = -3.32 and *E*(Na,1) = -3.28 eV. In addition to these sites the BVSE analysis reveals an insterstitial site *i* at about (0.359, 0.045, 0) as a local minimum with a somewhat higher site energy of *E*(Na,*i*) = -2.95 eV.

The lowest energy hop should be from a Na(1) site to one of two adjacent *i* sites, as their connection requires an activation energy of E_A 0.35 eV (Table 4). With a slightly higher activation energy of 0.42 eV the interstitial site can also be reached from Na(2). Thereby sodium ions with this activation energy can move within a local pathway loop [Na(1)-i-Na(2)-i-Na(1)-i-Na(2)-i]. With an activation energy of 0.60 eV the Na^+ can then also hop from the *i* site of one local loop to the *i* site within a neighboring loop, interconnecting local pathways to a two-dimensional continuous pathway for *dc* ionic conductivity in good agreement with the experimental finding of an activation energy of 0.61 eV for ionic conductivity in this compound [1].

Table 4. Characteristic sites and their interconnections in the BVSE landscape of $Na_2CoP_2O_7$.

Site	Site energy /“eV”	Classification
Na(2)	-3.32	equilibrium site
Na(1)	-3.28	equilibrium site
i	-2.95	interstitial site at about (0.359, 0.045, 0)
Connection	**Type of paths**	**Scaled E_A***
Na(1)-i	local path i-Na(1)-i	0.35 Ev
i-Na(2)	local pathway loop involving 2 Na(1), 2 Na(2), 4 i	0.42 eV
i-i	2D infinite paths by connection of local loops via i-i bridges	0.60 eV

**A static model excluding counterion relaxations inevitably overestimates activation energies for ion mobility, so the activation energies derived from such models have to be scaled down to yield realistic values. A scaling factor of about 0.42 was found to work approximately for a range of layered oxides; while for 3D network structures, where structural relaxations cost more energy and take more time a scaling factor of 0.8 appears appropriate.*

Figure 6 shows the lower energy sites regions where monovalent (Na +) cations can be displaced.

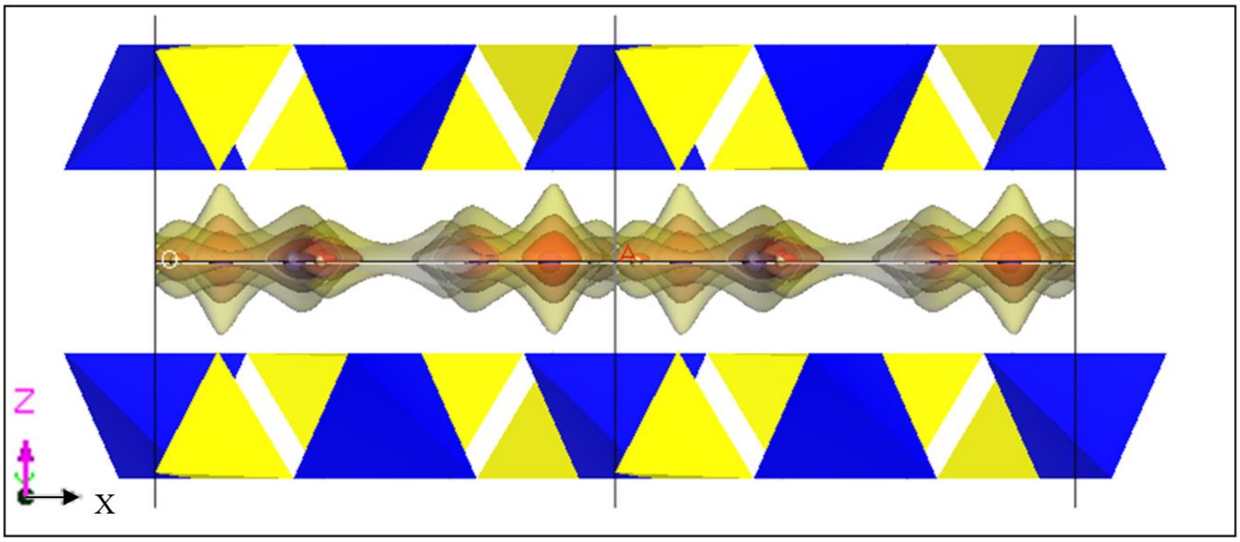

Figure 6. Na^+ pathways from the BVSE model calculations in the $Na_2CoP_2O_7$ material

4.4.2. Na transport pathways in $K_{0.86}Na_{1.14}CoP_2O_7$

For the description of pathways in mixed mobile cation materials, here K^+/Na^+, it is best to create local structure models with the respective overall composition, and random occupancies of the K/Na on the respective sites. Here, we discuss pathways in a 2×2×1 supercell with 16 A1 and 16 A2 sites: 5 K / 11 Na on site A1; 9 K / 7 Na on site A2 corresponding to the composition of the crystal structure listed in Table 2. The random distribution led to a 6 K : 10 Na ratio in the layer around $z = 0$ and a 7 K : 9 Na ratio in the layer around $z = ½$. To retain the close correlation to the refined structure data, no structural relaxation of the anion arrangement around this randomly assigned alkali distribution was conducted.

The resulting two pathway layers shown in Figure 7 (b) and (c) visualize the key effects of the mixed alkali doping compared to the paths in single alkali $Na_2CoP_2O_7$ [1] (Fig. 7a): In the layer shown in Figure 7b, the absolute energy to overcome bottlenecks between Na sites are raised in energy slightly (by 0.05-0.07 eV), yet this effect is compensated by the higher site energies of the equilibrium (and interstitial) sites. Thereby for the composition corresponding to 6 K:10 Na ratio in this layer and the specific arrangement of K^+ ions a 2D pathway should occur for a hardly changed (in the given case even slightly lower activation energy), but the resulting network of pathways is much more fragile relying on just a few low energy connections (compared to the much more redundant and thus robust pathway network for 16 Na/0 K seen in Figure 7a). This will reduce the absolute conductivity and the Na^+ ion will in practice not only follow this lowest energy path but also have to overcome some higher energy barriers.

For the case 7 K/ 8 Na realized in the second alkali layer of the local structure model (shown in Figure 7c), it turns out that there is no long range Na^+ migration pathway at all even at very high energies due to the blocking of paths by the specific K^+ arrangement. So this entire layer of the supercell will in the model not contribute to the Na^+ conductivity.

In a real structure we would see a mixture of both extreme cases and a wide range of intermediate ones.

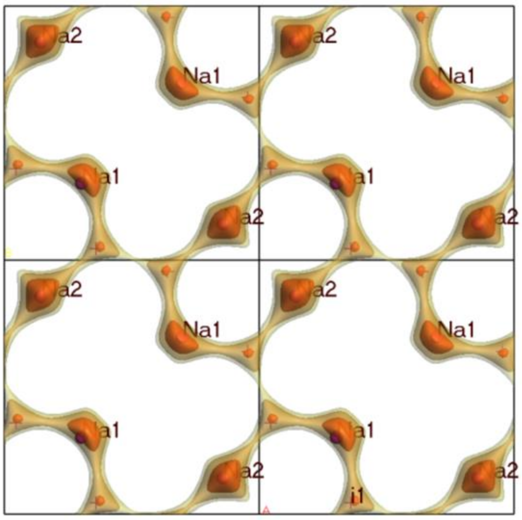

(a) $Na_2CoP_2O_7$ ($z \approx 0$)

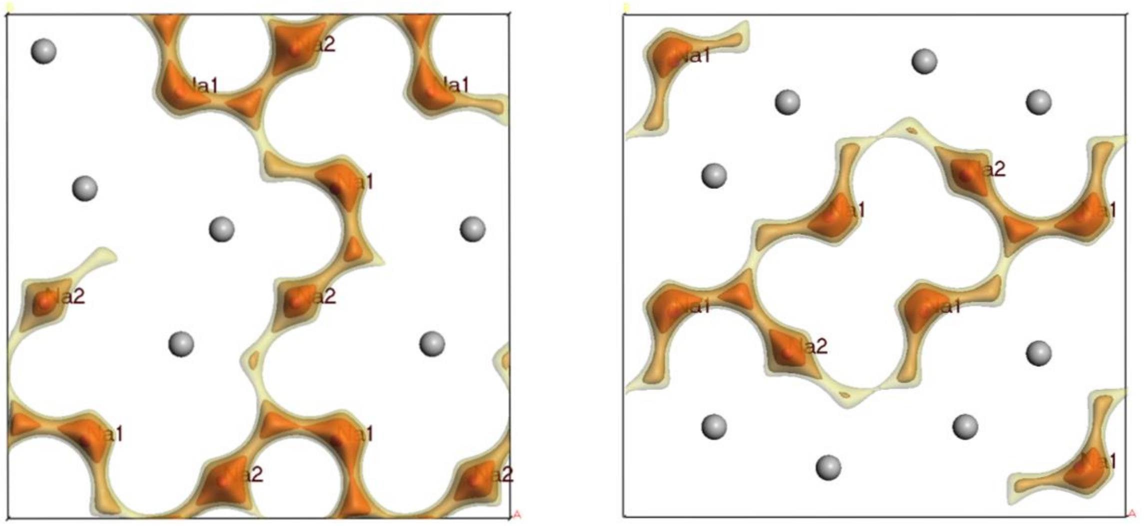

(b) $K_{6/8}Na_{10/8}CoP_2O_7$ ($z \approx 0$) (c) $K_{14/16}Na_{18/16}CoP_2O_7$ ($z \approx 1/2$)

Figure 7. (a) Bond valence site energy model of Na^+ ion transport pathways in $Na_2CoP_2O_7$ [1]. Three isosurfaces of constant Na site energy mark corresponding to Na sites as regions of lowest site energy (dark), local pathways (intermediate) and two-dimensional continuous pathways (light isosurface) are superimposed. Na(1) and Na(2) sites are marked by labels, interstitial sites by a crosses. The projection spans over 2 unit cells in *a* and *b* direction to clarify the local pathway loop, and from z = ¼ to z = -¼ . The identical 2D pathway around z = ½ remains separated from this pathway even for very high activation energies. Graphs (b) and (c) show the corresponding pathways for the same energy thresholds in two layers of a local $K_{14/16}Na_{18/16}CoP_2O_7$ structure model based on the structure refinement in Table 2 and a random alkali ion distribution approximating the observed site occupancies. Sites occupied by K^+ ions are marked as grey spheres.

Thereby a wider distribution of local activation energy barriers will be realized leading overall to an increase of activation energy of the rate limiting step and a significantly lower absolute value of the conductivity due to the elimination of pathway branches by blocking K^+ ions. As K^+ are the minority ions here, blocking of the anyway lower K^+ ion transport by Na^+ will be even more prominent and practically no K^+ conductivity should be observed for the 7 K/8 Na composition.

5. CONCLUSION

In this work, a new sodium-potassium cobalt diphosphate compound, $K_{0.86}Na_{1.14}CoP_2O_7$, has been synthesized by solid state reaction. The distribution character of the two alkali cations in the framework interstices has been investigated by single-crystal X-ray diffraction in a sample which its formula determined to be. The bond valence and charge-distribution validation tools are used to confirm the structural model. The title compound crystallizes in the tetragonal system, space group P42/mnm with a=7.808(3) Å, c=10.757(3) Å. The structure can be described as layered since it is formed by slabs of $[CoP_2O_7]^-_\infty$ with Na/K alkali-cations lying between the layers.

Adequate milling procedures using agate jars and planetary milling apparatus, attended by appropriate sintering, permit the control of the ceramic relative density. The electrical properties of $K_{0.86}Na_{1.14}CoP_2O_7$ sample with relative density of 83% were studied using complex impedance spectroscopy. The electrical conductivity is rather low, 8.26×10^{-7} $S.cm^{-1}$ at 390°C and the Arrhenius energy activation is 1.34 eV. The bond-valence site energy reveals that the ionic conductivity of the $K_{0.86}Na_{1.14}CoP_2O_7$ compound is probably ensured by Na^+ in the interlayer space.

ACKNOWLEDGEMENTS
The authors extend their appreciation to the Deanship of Scientific Research at King Khalid University for funding this work through research groups program under grant number R.G.P.1/25/38.

SUPPORTING DATA
CIF file containing more details of the crystal structure was deposited in the Cambridge Crystallographic Data Centre (CCDC), 12 Union Road, Cambridge CB2 1EZ, UK; Fax: +44(0)1223-762911; email: deposit@ccdc.cam.ac.uk] (or at www.ccdc.cam.ac.uk/conts/retrieving.html) on quoting the deposit numbers CCDC918441 and 918442.

References

1. F. Sanz, C. Parada, J.M. Rojo, C. Ruiz-Valero, R. Saez-Puche, *J. Solid State Chem*., 145 (1999) 604-611.
2. F. Erragh, A. Boukhari, B. Elouadi, E.M. Holt, *J. Cryst. Spectrosc.,* 21(3) (1991) 321-326.
3. A. Ben Rhaiem, F. Hlel. K. Guidara. M. Gargouri. *J. Alloy. Comp*., 485 (2009) 718-723.
4. R. Marzouki, A. Guesmi, M.F. Zid, A.Driss, *Crystal Structure Theory and Applications, 1* (2013) 68-73.
5. I. Belharouak, P. Gravereau, C. Parent, J.P. Chaminade, E. Lebraud, G. Le Flem, *J. Solid State Chem*.,152 (2000) 466-473.
6. I. Belharouak, C. Parent, P. Gravereau, J.P. Chaminade, G. Le Flem, B. Moine, *J. Solid State Chem.,* 149(2) (2000) 284-291.
7. F. Erragh, A. Boukhari, A. Sadel, E.M. Holt*, Acta Crystallogr*., C54 (1998) 1373-1376.
8. E. Hafidi, M. El Omari, M. El Omari, A. Bentayeb, J. Bennazha, A. El Maadi, M. Chehbouni, *Arabian J. of Chem*., 6(3) (2013) 253-263.
9. A. Guesmi, A. Driss, *J. Soc. Chim. Tunisie*, 4 (2002) 1675-1683.
10. V.I. Mokeeva, E.S. Makarov, *Geokhimiya*, 10 (1979) 1541-1544.
11. M. Gabelica-Robert, E.F. Bertaut, *C.R. Acad. SC. Paris*, t. 293 Série II (1981) 497-499.
12. A. J. M. Duisenberg, *J. Appl. Crystallogr*., 25 (1992) 92-96.
13. J. Macíček, A. Yordanov*, J. Appl. Crystallogr*., 25 (1992) 73-80.
14. A.C.T. North, D.C. Phillips, F.S. Mathews, *Acta Crystallogr*., A 24 (1968) 351-359.
15. G.M. Sheldrick (2008). *Acta Cryst*., A64, 112-122.
16. L.J. Farrugia, *J. Appl. Crystallogr*., 32 (1999) 837-838.
17. K. Brandenburg, M. Berndt (2001) Diamond Version 2.1. Crystal Impact. Bonn.
18. I.D. Brown (2002) The Chemical Bond in Inorganic Chemistry- The Bond Valence Model. IUCR Monographs on Crystallography. 12. Oxford University Press.
19. S. Adams (2003) softBV, University of Göttingen. Germany. http://www.softBV.net.
20. D. Mazza, S. Ronchetti, O. Bohnke, H. Duroy, J.L. Fourquet, *Solid State Ionics*, 149 (1-2) (2002) 81-88.
21. S.Adams, *Solid State Ionics,* 177 (2006) 1625-1630.

22. S.Adams, *Appl. Energy,* 90 (2012) 323-328.
23. D. Mazza, *J. Solid State Chem*., 156 (2001) 154-160.
24. Y. Ben Smida, R. Marzouki, A. Guesmi, S. Georges, M.F. Zid, *J. Solid State Chem*., 222 (2015) 132-139.
25. M. Avdeev, M. Sale, S. Adams, R. Prasada Rao, *Solid State Ionics,* 225 (2012) 43-46.
26. S. Adams, R. Prasada Rao, *Phys. Status Solidi,* A 208 (2011) 1746-1753.
27. S. Adams, R. Prasada Rao, *Atom Indonesia,* 36 No.3 (2010) 95-104.
28. M. Nespolo (2001) CHARDIT-IT, CRM2, University Henri Poincaré Nancy. France.
29. M. Nespolo, G. Ferraris, G. Ivaldi, R. Hoppe, *Acta Cryst*., B57 (2001) 652-664.
30. V. Petricek, M. Dusek, L.Palatinus, Jana, The crystallographic computing system, Institute of Physics, Praha, Czech Republic (2006).
31. R. Marzouki, A. Guesmi, S. Georges, M. F. Zid, A. Driss, *J. Alloys Compd*., 586 (2014) 74-79.
32. D. Johnson, 1990-2007, Zview version 3.1c. Scribner Associates. Inc.
33. I.M. Hodge, M.D. Ingram, A.R. West, *J. Electroanal. Chem*., 74 (1976) 125-143.
34. N. Dridi, A. Boukhari, J. M. Réau, E. Arbib, E.M. Holt, *Solid State Ionics,* 127 (2000) 141-149.
35. N. Dridi, A. Boukhari, J.M. Réau, E. Arbib, E.M. Holt, *Mater. Lett*., 47 (2001) 212-218.
36. R. Marzouki, A. Guesmi, M.F. Zid, A. Driss, *Ann. Chim. Sci. Mat*., 2013, 38 (3-4), 117-129.
37. Y. Ben Smida, R. Marzouki, S. Georges, R. Kutteh, M. Avdeev, A. Guesmi, M. F. Zid, *J. Solid State Chem*., 239 (2016) 8-16.
38. R. Nasri, R. Marzouki, S. Georges, S. Obbade, M. F. Zid, *Turk. J. Chem*., In Press doi:10.3906/kim-1801-89.